PHYSICAL REVIEW B **90**, 085105 (2014)

# Coexistence and competition of multiple charge-density-wave orders in rare-earth tritellurides

B. F. Hu,[1,2] B. Cheng,[2] R. H. Yuan,[2] T. Dong,[2] and N. L. Wang[2,3,4]

[1]*Key Laboratory of Neutron Physics, Institute of Nuclear Physics and Chemistry, China Academy of Engineering Physics, Mianyang 621900, China*

[2]*Beijing National Laboratory for Condensed Matter Physics, Institute of Physics, Chinese Academy of Sciences, Beijing 100190, China*

[3]*Collaborative Innovation Center of Quantum Matter, Beijing, China*

[4]*International Center for Quantum Materials, School of Physics, Peking University, Beijing 100871, China*

(Received 17 February 2014; revised manuscript received 17 July 2014; published 7 August 2014)

The occurrences of collective quantum states, such as superconductivity (SC) and charge- or spin-density waves (CDWs or SDWs), are among the most fascinating phenomena in solids. To date, much effort has been made to explore the interplay between different orders, yet little is known about the relationship of multiple orders of the same type. Here we report optical spectroscopy study on CDWs in the rare-earth tritelluride compounds $R\mathrm{Te}_3$ ($R =$ rare-earth elements). Besides the prior reported two CDW orders, the study reveals unexpectedly the presence of a third CDW order in the series, which evolves systematically with the size of $R$ element. With increased chemical pressure, the first and third CDW orders are both substantially suppressed and compete with the second one by depleting the low-energy spectral weight. A complete phase diagram for the multiple CDW orders in this series is established.

DOI: 10.1103/PhysRevB.90.085105 PACS number(s): 71.45.Lr, 78.20.−e, 78.30.Er

## I. INTRODUCTION

Charge-density-wave (CDW) states in low-dimensional electronic systems are among the most actively studied phenomena in condensed matter physics. Most CDW states are driven by the nesting topology of Fermi surfaces (FSs), i.e., the matching of sections of FS to others by a wave vector $\boldsymbol{q} = 2\boldsymbol{k}_F$, where the electronic susceptibility has a divergence [1,2]. A single-particle energy gap opens in the nested regions of the FSs at the transition, which leads to the lowering of the electronic energies of the system. Coupled to the lattice by electron-phonon interactions, the development of CDW state also causes a lattice distortion with the superstructure modulation wave vector matching with the FS nesting wave vector.

The family of rare-earth tritelluride $R\mathrm{Te}_3$ ($R$ being an element of the lanthanide family) presents an excellent low-dimensional model system to study the effect of FS nesting-driven CDW formation. $R\mathrm{Te}_3$ has a layered structure consisting of alternate stacking of the insulating $R$Te slab and the conducting Te only double planes along $b$ axis [3,4]. The FSs are strongly two-dimensional (2D) cylindrical like and exhibit nesting instabilities, leading to CDW ground states [5–7]. Interestingly, the CDW properties can be well tuned by choosing different elements of the lanthanide series. As the lanthanide 4$f$ electrons are far below the Fermi level, the major effect of changing different lanthanide element, without the entanglement of charge doping effect, is to exert chemical pressure [8–10]. By moving through the series from La to Tm, the increasing occupation of 4$f$ orbital leads to a decrease of the ion radii and the lattice parameters [9]. For $R\mathrm{Te}_3$, an incommensurate CDW ground state with a wave vector $\boldsymbol{q}_1 \approx 2/7\, \boldsymbol{c}^*$ was commonly observed [8,9]. For the four heavy rare-earth $R\mathrm{Te}_3$ ($R =$ Tm, Er, Ho, Dy) compounds, the development of a second CDW order, with the wave vector $\boldsymbol{q}_2 \approx 1/3\, \boldsymbol{a}^*$ perpendicular to the first one, was revealed and well documented [10–12].

In our previous optical spectroscopy study on $\mathrm{CeTe}_3$ and $\mathrm{TbTe}_3$, we also observed a clear, though weak, CDW energy gap feature developing below roughly 200 K, besides the major energy gap structure at higher energy [13,14], suggesting presence of another CDW order even in the light and intermediate rare-earth tritelluride compounds. However, the gap amplitude does not follow the trend observed for the four heavy rare-earth $R\mathrm{Te}_3$ compounds [7]. Those findings were extremely puzzling and motivated us to conduct further systematic study. In this work, we report the in-plane optical study on all of the eleven $R\mathrm{Te}_3$ ($R =$ La–Nd, Sm, Gd–Tm) compounds. The measurement clearly reveals the coexistence of multiple CDW orders in all members of $R\mathrm{Te}_3$ family. Besides the prior reported two ones, our optical study unexpectedly discovers the presence of a third CDW order in the series. The energy gaps observed previously in $\mathrm{CeTe}_3$ and $\mathrm{TbTe}_3$ at lower energies actually belong to the third CDW order, which had never been reported by any other probes before. The first and third CDW orders exhibit much similar systematic evolution as a function of $R$ and cooperate with each other while both compete with the second CDW order. We suggest that the third CDW order arises from the bilayer splitting, which lifts the degeneracy of conduction bands of double Te sheets. A complete phase diagram of CDW energy gaps versus lanthanide elements was established for the $R\mathrm{Te}_3$ compounds.

## II. EXPERIMENT AND RESULTS

The single crystals in the present study were grown by a self-flux method with a molar ratio $R$:Te = 1:40 in a procedure the same as in reference 13. The optical reflectance measurements were conducted on the Bruker IFS 80 v/s spectrometer in a frequency range from 40 $\mathrm{cm}^{-1}$ to 25 000 $\mathrm{cm}^{-1}$. An *in situ* gold and aluminium overcoating technique was used to get the reflectivity $R(\omega)$ [15]. The real part of the conductivity spectra $\sigma_1(\omega)$ was obtained through the Kramers-Kronig transformation of $R(\omega)$. A Hagen-Rubens relation was used in the low-frequency extrapolation and in the high-frequency part a constant value extrapolation was used up to 100 000 $\mathrm{cm}^{-1}$, above which an $\omega^{-4}$ relation was employed.

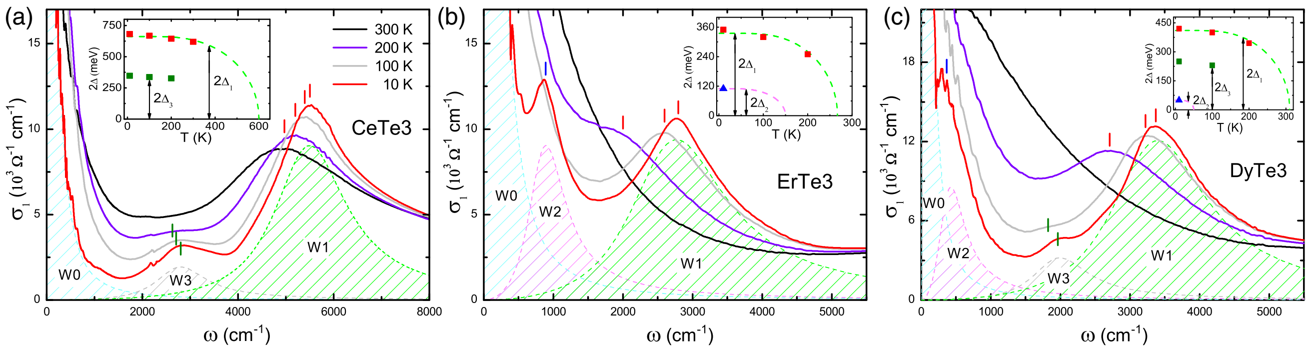

FIG. 1. (Color online) Temperature dependent optical conductivity $\sigma_1(\omega)$ of (a) $CeTe_3$, (b) $ErTe_3$, and (c) $DyTe_3$. The fitting curve of each Lorentz oscillation mode at 10 K, as well as that of the Drude resonance, was plotted at the bottom. The corresponding spectral weight, *W0* (Drude), *W1* (gap 1), *W2* (gap 2), and *W3* (gap 3), were revealed by the dashed area. The gap sizes were indicated by the short vertical lines. (Insets) The CDW gaps' sizes as functions of T. The dashed lines show the gap function $2\Delta(T)$ based on the weak coupling mean-field theory and serve as a guide to the eye. The values $2\Delta(T)$ are scaled to the experimental results and adjusted so as to fit the gap sizes at different temperatures.

We have performed temperature dependent optical measurements on all of the eleven compounds in rare-earth tritelluride family $RTe_3$ ($R =$ La–Nd, Sm, Gd–Tm). Figure 1 shows temperature dependent optical spectra of three representative compounds $CeTe_3$, $ErTe_3$, and $DyTe_3$. We note that the development of multiple peak features at low temperature not only appears in the heavy rare-earth compounds but also emerges in the light ones. In $DyTe_3$, even three peaks are present in the conductivity spectrum at 10 K. Meanwhile, the residual Drude component narrows significantly. The data yield explicit evidence for the opening of multiple partial CDW gaps on FSs [12,13]. Usually, the peak position was used to estimate the CDW energy gap due to the spectral weight transfer from the free carrier response to the energy scale just above the energy gap of $\hbar\omega = 2\Delta$. The formation of the peak or maximum in $\sigma_1(\omega)$ is caused by both the density of state and the type I coherence factor effect [1,2]. To quantify the discussions, a Drude-Lorentz model was employed to extract the CDW gap sizes and the relevant spectral weight [12–14], as will be presented below in detail.

Figure 2 shows the optical spectra of the whole $RTe_3$ series at two representative temperatures 10 and 300 K. For each compound, multiple suppressions in $R(\omega)$ arise at 10 K and simultaneously multiple peaks appear in $\sigma_1(\omega)$. Both features suggest the formations of CDW orders. The CDW energy gaps were indicated by the short vertical lines and could be obviously categorized into three groups: gap 1, gap 2, and gap 3. In each group, the gap amplitude exhibits monotonic evolution as a function of chemical pressure ($R$ element). The Drude-Lorentz fitting results, as well as the CDW transition temperatures, were collected in Table I and a direct view of the systematic evolutions as functions of $R$ was given in Fig. 3. At the lowest measurement temperature, gap 1 exists in the whole $RTe_3$ series, gap 2 only arises in the four heavy rare-earth compounds, while gap 3 survives from the light to relatively heavy ones. Specially in $DyTe_3$, all the three gaps coexist. The first and second CDW orders occur with transition temperatures $T_{c1} = 310$ K and $T_{c2} = 52$ K, respectively [10]. In our optical measurements, the feature of gap 3 arises between 100 and 200 K, while the transition temperature has not yet been determined by other probes. The three CDW orders seem to coexist also in the neighboring compound $TbTe_3$, as a recent synchrotron x-ray diffraction study on $TbTe_3$ indicated the presence of the second CDW order with transition temperature $T_{c2} = 41$ K [16]. According to gap 2's evolution as a function of $R$, the gap energy scale should be less than 50 meV. It is rather close to the sizable Drude component and possesses much smaller spectral weight. As a consequence, the gap structure may become blurred in our optical measurement.

On traversing the lanthanide series from light rare-earth to heavier ones, the lattice parameter $a$ decreases monotonically and thus chemical pressure oppositely increases [9,10]. It is noteworthy that the $RTe_3$ compounds are ideal platforms for the study of (chemical) pressure tuned variations since doping entanglement is completely absent [10,17]. The $4f$ electrons hide in the inner shell and the relative bands are far below the Fermi level [7], which have little influence over the FS properties. In Fig. 3(a), we note that gaps 1 and 3 show much similar monotonic evolutions and both suffer substantial suppressions with increased chemical pressure. For the heavy rare-earth compounds $HoTe_3$, $ErTe_3$, and $TmTe_3$, gap 3 is completely suppressed. Meanwhile, gap 2 suddenly arises and becomes larger against the other two ones from $DyTe_3$ to $TmTe_3$. The transition temperatures $T_{c1}$ and $T_{c2}$ hold nearly the same evolution trend with the CDW gaps [10]. In the spectral weight plot [Fig. 3(d)], *W1* and *W3* manifest little variations versus $a$ for the light rare-earth compounds. With the emergence of gap 2, both undergo sudden depressions. The CDW versus $a$ plot establishes a complete electronic phase diagram in $RTe_3$ series, which clearly reveals the coexistence and competition of multiple CDW orders.

Gap 1 is relative to the first CDW order [5,7,13,18], which occurs with an incommensurate wave vector $\boldsymbol{q}_1 \approx 2/7\,\boldsymbol{c}^*$ [8,9]. The transition temperature $T_{c1}$ was plotted in Fig. 3(c). The second CDW order with a wave vector $\boldsymbol{q}_2 \approx 1/3\,\boldsymbol{a}^*$, which is also incommensurate, only arises in the four heavy rare-earth compounds from $DyTe_3$ to $TmTe_3$ and is responsible for gap 2 [10–12]. The FS nesting conditions responsible for the two

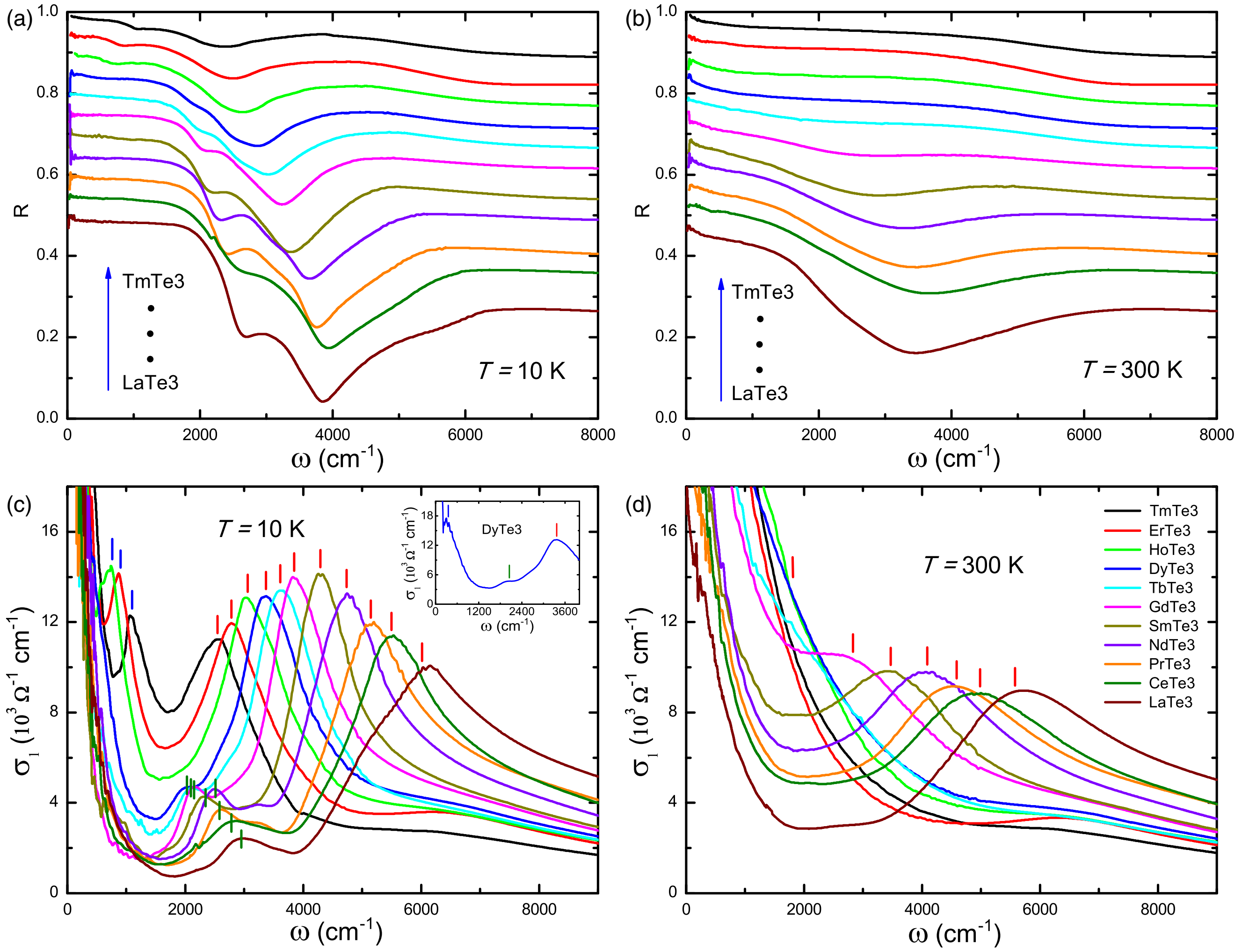

FIG. 2. (Color online) (a) The in-plane optical reflectivity $R(\omega)$ of $R\mathrm{Te}_3$ at 10 K. (b) The same plot as (a) at 300 K. In both panels, each $R(\omega)$ curve, except for that of $\mathrm{TmTe}_3$, was shifted away vertically from its neighbors by 0.05 for clarity. (c) The optical conductivity $\sigma_1(\omega)$ of $R\mathrm{Te}_3$ at 10 K. For each compound in $R\mathrm{Te}_3$ series, it clearly indicates formations of multiple CDW energy gaps at 10 K, which manifest strongly systematic evolutions across the series. According to the peak position and evolution behavior, the multiple energy gaps could be classified into three groups. The gap sizes were indicated by the short vertical lines in red (gap 1), blue (gap 2), and olive (gap 3). The inset shows the three gap features in $\mathrm{DyTe}_3$. (d) The optical conductivity $\sigma_1(\omega)$ of $R\mathrm{Te}_3$ at 300 K. For the light rare-earth compounds from $\mathrm{LaTe}_3$ to $\mathrm{TbTe}_3$, the first energy gap feature is still present at 300 K.

orders were illustrated in Fig. 4 [6,10,19]. By contrast, except for our earlier optical probes on $\mathrm{CeTe}_3$ and $\mathrm{TbTe}_3$ [13,14], remarkably, nothing about gap 3 was known to date. Since the gap amplitude and its evolution in the systems have been well established, the gap origin and its position in $\boldsymbol{k}$ space are highly desired. Here, we would like to stress that gap 3 does not belong to the other two known CDW orders. In the spin-density-wave (SDW) transition in Fe-based superconducting parents, two distinct energy scales were identified below $T_c$ [20], which were explained to arise from the gapping of different FS

TABLE I. Single-particle gap $2\Delta$ and transition temperature $T_c$ of the CDW orders in $R\mathrm{Te}_3$ compounds. The values in the top three rows and in the fourth one are the CDW single-particle gaps at 10 and 300 K, respectively. The transition temperatures were defined by the transport anomaly in $\rho(T)$ in Ref. [10]. The transition temperatures $T_{c3}$s have not yet been reported.

| | $\mathrm{LaTe}_3$ | $\mathrm{CeTe}_3$ | $\mathrm{PrTe}_3$ | $\mathrm{NdTe}_3$ | $\mathrm{SmTe}_3$ | $\mathrm{GdTe}_3$ | $\mathrm{TbTe}_3$ | $\mathrm{DyTe}_3$ | $\mathrm{HoTe}_3$ | $\mathrm{ErTe}_3$ | $\mathrm{TmTe}_3$ |
|---|---|---|---|---|---|---|---|---|---|---|---|
| $2\Delta_1$(10 K) | 750 | 680 | 640 | 590 | 530 | 480 | 450 | 420 | 380 | 350 | 320 |
| $2\Delta_2$(10 K) | – | – | – | – | – | – | – | 50 | 90 | 110 | 140 |
| $2\Delta_3$(10 K) | 370 | 350 | 320 | 310 | 290 | 270 | 260 | 250 | – | – | – |
| $2\Delta_1$(300 K) | 700 | 620 | 570 | 510 | 430 | 350 | 220 | – | – | – | – |
| $T_{c1}$ | – | – | – | – | 416 | 377 | 336 | 310 | 288 | 267 | 244 |
| $T_{c2}$ | – | – | – | – | – | – | – | 52 | 110 | 157 | 180 |

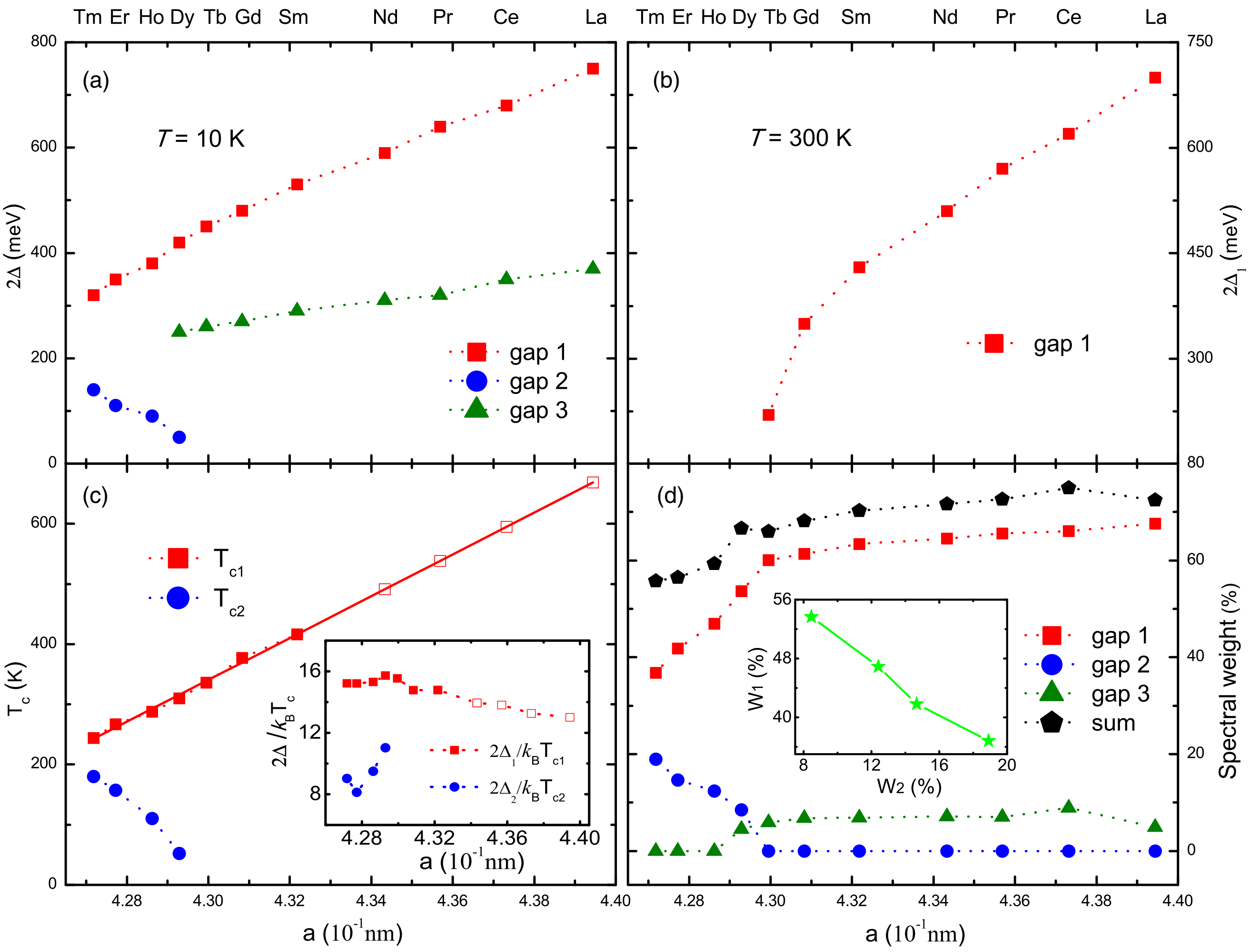

FIG. 3. (Color online) (a) and (b) CDW single-particle gap 2Δ at 10 and 300 K, respectively. (c) The transition temperatures $T_{c1}$ and $T_{c2}$ [10]. For the four light rare-earth compounds from LaTe$_3$ to NdTe$_3$, $T_{c1}$s are above 450 K and have not yet been determined by experimental probes. The four values, which were plotted in open squares, were obtained by the fitting and extrapolation of the other compounds' transitions. The solid straight line is an indication of the linear fit. The inset shows the ratios $2\Delta/k_BT_c$s for the first and second CDW orders. (d) Chemical pressure ($R$) dependence of the spectral weight lost to each CDW gap (*W1*, *W2*, *W3*), expressed as a percentage of that of the total free carriers in normal state. The total spectral weight lost in CDW states is plotted in black pentagons. The inset shows the plot of $W_1$ against $W_2$, which clearly demonstrates the anticorrelation of the two quantities. The lattice parameter $a$ was obtained in reference 9 at 300 K, for which the relative $R$Te$_3$ compounds were indicated on the top of the figures. The dotted lines were employed as a guide to the eye.

sheets. Here the possibility was ruled out because the three kinds of energy gaps all develop at different temperatures. In our temperature-dependent optical measurements, the features relative to gap 3 all emerge below 300 K. Moreover, gap 3, appearing between 2000 cm$^{-1}$ to 3000 cm$^{-1}$, can not be ascribed to the CDW collective excitations, either the phase mode or the amplitude mode. The former is usually pinned in the microwave or millimeter-wave spectral range by impurity or lattice imperfections [1,2,21], while the latter is much lower than the unrenormalized phonon frequency at Kohn anomaly [2,22]. Furthermore, the scenario of pseudogap character prior to the underlying second CDW transition, due to fluctuation effect [2,10,12], could also be excluded since gaps 2 and 3 exhibit the opposite evolution across the lanthanides series and both features are present in DyTe$_3$. Therefore gap 3 represents a new or third CDW order, of which the nesting condition is expected.

The crystal structure [3,4] and schematic FS of $R$Te$_3$ are displayed in Fig. 4 [6,7,10,11,19]. The plot of the FSs has been simplified for the purpose of illustrating the nesting conditions. According to the band structure calculation on the 3D crystal structure with the employment of the linear muffin-tin orbital (LMTO) method, the FS consists of three parts contributed by the $p_x$ and $p_z$ orbitals of metallic Te layers: Γ-centered squarelike FS, $M$-centered FS mainly in the second Brillouin zone, and $X/Z$-centered small-size FS. Here, we have unfolded the third part into the second Brillouin zone. Then, the FSs could be approximately viewed as two Γ-centered pieces: inner and outer ones [6,7]. The 4$f$ electrons of rare-earth $R$ are far below the Fermi level and have little effect on $E_F$. Since there are two conducting Te planes between the insulating $R$Te slabs in the crystal structure [as can be seen from Fig. 4(a)], the interlayer coupling of the two neighboring metallic Te layers would break the degeneracy of conduction

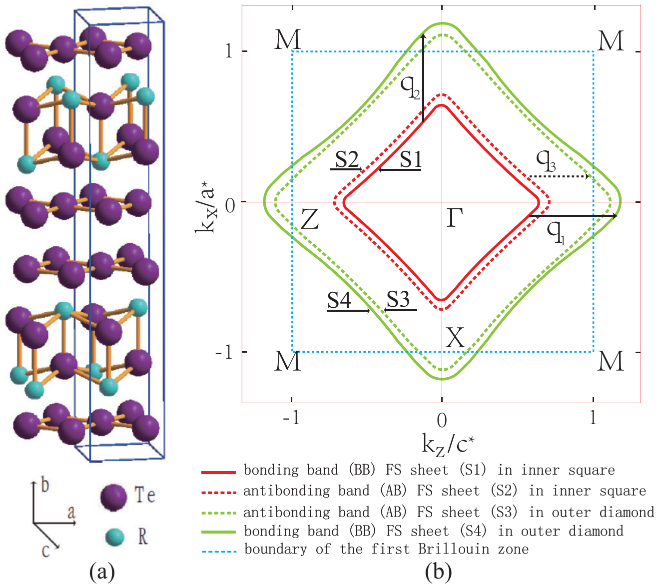

(a)
(b)

FIG. 4. (Color online) (a) Crystal structure of *R*Te$_3$. (b) Schematic diagram of FSs of *R*Te$_3$. The FSs, showing little dispersion along $\boldsymbol{b}^*$ axis, are projected onto the Γ-*X*-*Z* plane ($\boldsymbol{k}_y = 0$). The FS contours consist of two Γ-centered pockets, the holelike inner square (in red) and the electronlike outer diamond (in green) [6,10]. Due to coupling of two neighboring Te layers, each contour splits into two parallel sections (bilayer splitting). The amplitude of bilayer splitting varies on the FS, which is schematically illustrated by the separated distance. The bilayer splitting reaches maximum near the corner ($\delta \approx 0.03\mathbf{c}^*$) [7]. The nesting wave vectors are also illustrated. For clarity, only Γ-centered FSs are displayed.

band and yields two nearly parallel FS crossings: bonding band (BB) and antibonding band (AB), which is usually called bilayer splitting [6,7,10,19]. Then the FSs are all double-wall like. It is noted that the outer FSs come from the band folding effect due to the fact that the real three-dimensional (3D) lattice structure actually doubles the unit cell of Te square lattice of the Te layers along its diagonal direction [7], then the bilayer splitting of inner FSs (S1 and S2) and the outer FSs (S3 and S4) are just opposite. Since S1 and S2 are nearly parallel and have quite similar FS topology, and the same case applies to S3 and S4, the nesting between the inner square and outer diamond, which is along $\boldsymbol{c}^*$ axis, would have two possible selections: (a) S1 nests S3 and S2 nests S4, (b) S1 nests S4 and S2 nests S3. In case (a), the nesting takes place between two different bands (interband nesting between BB and AB) and leads to a single nesting wave vector, and thus a single CDW transition. It is reminiscent of the blue bronze which, owning two partially filled bands and thus four FS sheets, has only one CDW and undergoes a metal-semiconductor transition [23,24]. In case (b), the nesting happens between the two FS sheets within each band (intraband nesting within BB and AB), which implies two different nesting wave vectors and two separated CDW transitions, as well as two distinct CDW gap energy scales. Our study favors the latter case.

Angle-resolved photoemission spectroscopy (ARPES) measurements reveal that the FSs on both BB and AB bands, which locate near the corner along $\boldsymbol{c}^*$ axis, were completely removed at 10 K [7,11,18]. Meanwhile, two different energy gaps were observed on the two parallel band sheets, a larger gap on BB and the smaller on AB [7]. Therefore it could be concluded that the nesting within BB leads to the first CDW order and that in AB causes the third one. The two CDW orders both occur along $\boldsymbol{c}^*$ axis and the nesting vectors $\boldsymbol{q}_1$ and $\boldsymbol{q}_3$ differ very little since the bilayer splitting is rather small. The interpretation is supported by the recent studies of the single layer rare-earth ditelluride CeTe$_2$ [25], where only one CDW order was identified along $\boldsymbol{c}^*$ axis since the bilayer splitting is absent [6]. It is worth noting that Yao *et al.* have addressed the question of occurrence of just one ordering transition or two distinct ones, which was determined by the comparison of relevant energy scales $t_{\text{bil}}$ (responsible for the bilayer splitting) and the CDW gap $2\Delta$ [19]. The present work clearly indicates that in *R*Te$_3$ series bilayer splitting is of primary importance and it can result in separated CDW orders.

## III. DISCUSSION

Our optical study explicitly reveals the development of a third energy gap in *R*Te$_3$ series upon lowering $T$, which yields strong evidence for the existence of a new CDW order distinct from the prior two ones. Surprisingly, this order has never been identified by any other techniques before. In the magnetic susceptibility and transport probes, neither measurement observes a clear anomaly in consequence of formation of the third CDW order [10,26–28]. In Fig. 1, we notice that in contrast to the pronounced free carrier response and the sizable spectral weight of the other two orders, the peak signature ascribed to gap 3 is much less notable. In Fig. 3(d), we find that just a very small amount of electrons responds to the third CDW transition. Take CeTe$_3$ as an example. The spectral weight of total free carriers in the normal state is $W = W0 + W1 + W2 + W3$ and the percentage of the spectral weight lost to each CDW gap is $\Phi_i = W_i/W$. The fitting results show that $\Phi_1 \approx 66\%$, while $\Phi_3 \approx 8.9\%$, which means that about two-thirds of FSs were gapped away in the first CDW transition while in the third one the lost density of states (DOS) at $E_F$ is substantially reduced. The very small spectral weight of gap 3 gives us some clues to understand the discrepancy. In the magnetic susceptibility measurement of LaTe$_3$, $\chi$ exhibits constant diamagnetic behavior [26]. La and Te are both heavy atoms with many closed shell core electrons. They collectively contribute considerable diamagnetism, which overcomes the small Pauli paramagnetism of the free electron gas. For the other compounds in *R*Te$_3$, $\chi$ is dominated by the $4f$ electrons and exhibits Curie-Weiss paramagnetism [27,28]. The effect of little variation of DOS near $E_F$ due to the third CDW is significantly reduced. The notion could also apply to the transport measurement, where resistivity $\rho(T)$ is determined by several factors, e.g., Fermi velocity, scattering rate, and free carrier density. The reduction of DOS near $E_F$ might be compensated by the other two factors. As a consequence, this CDW order could have rather weak effect on $\rho(T)$ and the corresponding signature becomes obscured.

Since the bilayer splitting is very small, the two wave vectors $q_1$ and $q_3$, as well as their associated modulation periodicity, are very close to each other. Moreover, the scattering intensity of CDW superlattice peaks is several orders of magnitude smaller than that of the average structure Bragg peaks [10]. To distinguish between the first and third CDW orders becomes extremely hard in x-ray scattering measurement. In spite of this, we notice that the temperature-dependent integrated intensity of superlattice peak in $TbTe_3$ shows an evident dip near 150 K [10], which was considered as an experimental artifact by the authors. However, it is very likely that the feature actually signals the presence of the third CDW transition. In the early ARPES measurement, the removal gaps on the FS sheets connected by the nesting wave vector were claimed to be unequal [5], which is in sharp contrast to the identical results in the later ARPES probe [7]. The seemingly controversial results are most likely caused by the bilayer splitting, which was investigated in different resolution conditions.

$R\mathrm{Te}_3$ systems represent a kind of a rare compound, which experiences multiple CDW transitions. The other examples include $NbSe_3$ and $\eta$-$Mo_4O_{11}$. Both exhibit two incommensurate CDWs with $T_{c1} = 145$ K and $T_{c2} = 59$ K for $NbSe_3$ [29,30] and $T_{c1} = 109$ K and $T_{c2} = 30$ K for $\eta$-$Mo_4O_{11}$ [24]. Whereas $R\mathrm{Te}_3$ is quite striking in which as many as three distinct CDW orders emerge coincidentally. It will be very interesting to study the interplay and relationship among the three but the same type orders. In Fig. 3(a), we note that gaps 1 and 3 coexist in most compounds in the series and display a similar monotonic evolution from light rare earth to heavier ones. Since the CDW orders are nesting driven, certain difference in the nesting conditions for the two CDW orders should exist. It is noted that the AB actually exhibits stronger $\boldsymbol{b}^*$-axis dispersion (perpendicular to the conduction *ac* plane) and thus worse nesting conditions than BB [7,10]. Therefore BB bears much stronger CDW instability than AB. The gap amplitude and the affected spectral weight of the first CDW order on BB are both much larger than that of the third one on AB.

The second CDW order, which occurs in the four heavy rare-earth compounds, displays monotonic evolution opposite to the other two ones. The transition temperature $T_{c2}$, as well as the CDW gap, increases with enhanced chemical pressure, which is rather peculiar since pressure generally suppresses CDW transitions [17,31]. In Fig. 3(d), we notice that from $LaTe_3$ to $TbTe_3$, in which the second CDW order is absent, the lost spectral weight *W1* and *W3* display rather little variations. The rapid suppression of both values just coincides with the onset of the second CDW order. To examine the relationship of the orders, we plot *W1* versus *W2* in the inset. The two quantities show almost perfect linear anticorrelation in the four heavy rare-earth compounds. It explicitly demonstrates that the second CDW order competes with the other two ones for the low-energy spectral weight available for nesting. With increased chemical pressure, the amount of gapped FS by the first and third CDW orders reduces [7] and more intact FS is left to contribute to the second CDW transition [10].

For the four heavy rare-earth compounds, the second CDW order occurring perpendicular to the other two ones, a bidirectional checkerboard CDW ground state would arise [10,19]. It is reminiscent of the pseudogap state in high-$T_c$ cuprates, of which the origin has been long debated between the precursor superconducting paring gap and competing orders. In the former viewpoint, the pseudogap is believed to be the preformed Cooper pairs' gap before the coherence necessary for superconductivity (SC), which is rigidly tied to the superconducting phenomenon. In the latter point, the pseudogap is suggested to be a new phase, having no direct relationship with SC, which even competes and is harmful to SC. Though the origin is still under debate, there is growing evidence that the pseudogap arises from a checkerboard CDW order with perpendicular wave vectors close to $\mathbf{Q} = (\pm 2\pi/4, 0), (0, \pm 2\pi/4)$ [32–34]. The perpendicular CDW orders have fourfold symmetry [33,34] and occur simultaneously, while in the present systems the fourfold symmetry was broken due to the weakly orthorhombic structure [3,4]. The distinction between the perpendicular orders, nevertheless, tends to vanish with increased (chemical) pressures [9]. A fourfold checkerboard CDW is expected in the tetragonal lattice under sufficient high pressures.

## IV. CONCLUSIONS

To conclude, we performed a systematic optical spectroscopy study on CDWs in the eleven rare-earth tritelluride compounds $R\mathrm{Te}_3$ ($R$ = La–Nd, Sm, Gd–Tm). Besides the prior reported two CDW orders, the study reveals unexpectedly the presence of a third CDW order in the series which evolves systematically with the size of $R$ element. The puzzling energy gap features observed previously in the light rare-earth based compounds $CeTe_3$ and $TbTe_3$ at lower energies actually belong to this third CDW order. With increased chemical pressure, the first and third CDW orders are both substantially suppressed and compete with the second one by depleting the low energy spectral weight. We suggest that the third CDW order arises from the bilayer splitting, which lifts the degeneracy of conduction bands of double Te sheets. The study establishes a complete phase diagram for the multiple CDW orders in this series.

## ACKNOWLEDGMENTS

This work was supported by the National Science Foundation of China (11120101003, 11327806) and the 973 project of the Ministry of Science and Technology of China (2011CB921701, 2012CB821403).

---

[1] G. Grüner, Rev. Mod. Phys. **60**, 1129 (1988).
[2] G. Grüner, *Density Waves in Solids* (Addison-Wesley, Reading, MA, 1994).
[3] B. K. Norling and H. Steinfink, Inorg. Chem. **5**, 1488 (1966).
[4] E. DiMasi, B. Foran, M. C. Aronson, and S. Lee, Chem. Mater. **6**, 1867 (1994).
[5] G.-H. Gweon, J. D. Denlinger, J. A. Clack, J. W. Allen, C. G. Olson, E. DiMasi, M. C. Aronson, B. Foran, and S. Lee, Phys. Rev. Lett. **81**, 886 (1998).

[6] J. Laverock, S. B. Dugdale, Zs. Major, M. A. Alam, N. Ru, I. R. Fisher, G. Santi, and E. Bruno, Phys. Rev. B **71**, 085114 (2005).

[7] V. Brouet, W. L. Yang, X. J. Zhou, Z. Hussain, R. G. Moore, R. He, D. H. Lu, Z. X. Shen, J. Laverock, S. B. Dugdale, N. Ru, and I. R. Fisher, Phys. Rev. B **77**, 235104 (2008).

[8] E. DiMasi, M. C. Aronson, J. F. Mansfield, B. Foran, and S. Lee, Phys. Rev. B **52**, 14516 (1995).

[9] C. D. Malliakas and M. G. Kanatzidis, J. Am. Chem. Soc. **128**, 12612 (2006).

[10] N. Ru, C. L. Condron, G. Y. Margulis, K. Y. Shin, J. Laverock, S. B. Dugdale, M. F. Toney, and I. R. Fisher, Phys. Rev. B **77**, 035114 (2008).

[11] R. G. Moore, V. Brouet, R. He, D. H. Lu, N. Ru, J.-H. Chu, I. R. Fisher, and Z.-X. Shen, Phys. Rev. B **81**, 073102 (2010).

[12] B. F. Hu, B. Cheng, R. H. Yuan, T. Dong, A. F. Fang, W. T. Guo, Z. G. Chen, P. Zheng, Y. G. Shi, and N. L. Wang, Phys. Rev. B **84**, 155132 (2011).

[13] B. F. Hu, P. Zheng, R. H. Yuan, T. Dong, B. Cheng, Z. G. Chen, and N. L. Wang, Phys. Rev. B **83**, 155113 (2011).

[14] R. Y. Chen, B. F. Hu, T. Dong, and N. L. Wang, Phys. Rev. B **89**, 075114 (2014).

[15] C. C. Homes, M. Reedyk, D. A. Crandles, and T. Timusk, Appl. Opt. **32**, 2973 (1993).

[16] A. Banerjee, Yejun Feng, D. M. Silevitch, Jiyang Wang, J. C. Lang, H.-H. Kuo, I. R. Fisher, and T. F. Rosenbaum, Phys. Rev. B **87**, 155131 (2013).

[17] A. Sacchetti, C. L. Condron, S. N. Gvasaliya, F. Pfuner, M. Lavagnini, M. Baldini, M. F. Toney, M. Merlini, M. Hanfland, J. Mesot, J. H. Chu, I. R. Fisher, P. Postorino, and L. Degiorgi, Phys. Rev. B **79**, 201101(R) (2009).

[18] V. Brouet, W. L. Yang, X. J. Zhou, Z. Hussain, N. Ru, K. Y. Shin, I. R. Fisher, and Z. X. Shen, Phys. Rev. Lett. **93**, 126405 (2004).

[19] Hong Yao, John A. Robertson, Eun-Ah Kim, and Steven A. Kivelson, Phys. Rev. B **74**, 245126 (2006).

[20] W. Z. Hu, J. Dong, G. Li, Z. Li, P. Zheng, G. F. Chen, J. L. Luo, and N. L. Wang, Phys. Rev. Lett. **101**, 257005 (2008).

[21] M. Dressel and G. Grüner, *Electrodynamics of Solids* (Cambridge University Press, Cambridge, 2002).

[22] M. Lavagnini, M. Baldini, A. Sacchetti, D. Di Castro, B. Delley, R. Monnier, J.-H. Chu, N. Ru, I. R. Fisher, P. Postorino, and L. Degiorgi, Phys. Rev. B **78**, 201101 (2008).

[23] G. Travaglini, P. Wachter, J. Marcus, and C. Schlenker, Solid State Commun. **37**, 599 (1981).

[24] E. Canadell and M.-H. Whangbo, Chem. Rev. **91**, 965 (1991).

[25] Y. Huang, B. F. Hu, T. Dong, A. F. Fang, P. Zheng, and N. L. Wang, Phys. Rev. B **86**, 205123 (2012).

[26] N. Ru and I. R. Fisher, Phys. Rev. B **73**, 033101 (2006).

[27] N. Ru, J.-H. Chu, and I. R. Fisher, Phys. Rev. B **78**, 012410 (2008).

[28] Y. Iyeiri, T. Okumura, C. Michioka, and K. Suzuki, Phys. Rev. B **67**, 144417 (2003).

[29] J. Schäfer, Eli Rotenberg, S. D. Kevan, P. Blaha, R. Claessen, and R. E. Thorne, Phys. Rev. Lett. **87**, 196403 (2001).

[30] J. Schäfer, M. Sing, R. Claessen, Eli Rotenberg, X. J. Zhou, R. E. Thorne, and S. D. Kevan, Phys. Rev. Lett. **91**, 066401 (2003).

[31] A. Briggs, P. Monceau, M. Nunez-Regueiro, J. Peyrard, M. Ribault, and J. Richard, J. Phys. C: Solid State Phys. **13**, 2117 (1980).

[32] K. McElroy, D.-H. Lee, J. E. Hoffman, K. M. Lang, J. Lee, E. W. Hudson, H. Eisaki, S. Uchida, and J. C. Davis, Phys. Rev. Lett. **94**, 197005 (2005).

[33] J. X. Li, C. Q. Wu, and D. H. Lee, Phys. Rev. B **74**, 184515 (2006).

[34] W. D. Wise, M. C. Boyer, Kamalesh Chatterjee, Takeshi Kondo, T. Takeuchi, H. Ikuta, Yayu Wang, and E. W. Hudson, Nat. Phys. **4**, 696 (2008).